

## Electron dynamics of tip-tunable oxygen species on TiO<sub>2</sub> surface

Yuuki Adachi<sup>1</sup>, Ján Brndiar<sup>2</sup>, Huan Fei Wen<sup>1,3</sup>, Quanzhen Zhang<sup>1</sup>, Masato Miyazaki<sup>1</sup>, Sourbh Thakur<sup>2</sup>, Yasuhiro Sugawara<sup>1</sup>, Hongqian Sang<sup>4</sup>, YanJun Li<sup>1</sup>, Ivan Štich<sup>2,5,6</sup> & Lev Kantorovich<sup>7</sup>

The redox states of oxygen species on the surface of TiO<sub>2</sub> can be altered by electron tunneling by varying the applied bias voltage of an atomic force microscope tip. However, tunneling is stochastic in nature and typically requires ultra-low temperatures to obtain statistically significant data. Here, we use a highly sensitive fast atomic force microscopy setup to study redox transitions of oxygen atoms on a TiO<sub>2</sub> surface, in the form of reactive oxygen species and single-atom quantum dots, at 78 K. The fast and highly sensitive nature of our experimental setup enables a statistically necessary amount of data to be collected without having to resort to ultra-low temperatures. This enabled us to study multiple dots and provide insight into the electronic structure and correlation between the oxygen species, which are inaccessible by standard atomic force microscopy. We show that single-atom quantum dots exist in two charge states with drastically different conductance, with one being conducting and the other non-conducting.

<sup>1</sup>Department of Applied Physics, Osaka University, Suita, Osaka, Japan. <sup>2</sup>CCMS, Institute of Physics, Slovak Academy of Sciences, Bratislava, Slovakia. <sup>3</sup>Key Laboratory of Instrumentation Science and Dynamic Measurement, School of Instrument and Electronics, North University of China, Taiyuan, Shanxi, China. <sup>4</sup>Institute for Interdisciplinary Research, Jiangnan University, Wuhan, China. <sup>5</sup>Institute of Informatics, Slovak Academy of Sciences, Bratislava, Slovakia. <sup>6</sup>Department of Natural Sciences, University of Ss. Cyril and Methodius, Trnava, Slovakia. <sup>7</sup>Department of Physics, School of Natural and Mathematical Sciences, King's College London, London, UK. ✉email: [liyanjun@ap.eng.osaka-u.ac.jp](mailto:liyanjun@ap.eng.osaka-u.ac.jp); [ivan.stich@savba.sk](mailto:ivan.stich@savba.sk); [lev.kantorovitch@kcl.ac.uk](mailto:lev.kantorovitch@kcl.ac.uk)

Rutile  $\text{TiO}_2(110)$  surface is a prototypical transition metal oxide surface<sup>1</sup>, and adsorption and dynamics of oxygen on rutile  $\text{TiO}_2(110)$  and related materials has attracted a long-standing attention<sup>2–11</sup> due to its relevance to electron and hole mediated catalytic and photocatalytic reactions. It has been shown that oxygen atoms adsorbed as adatoms or molecular species on semiconducting surfaces may acquire several charge and spin states that can be manipulated by atomic force microscopy tip<sup>9,12–14</sup>. The zero-dimensional adatoms  $\text{O}_{ad}^{2-}$  or  $\text{O}_{ad}^-$  with the oxygen states confined within the  $\text{TiO}_2$  band gap form single-atom quantum dots (SaQDs)<sup>15–17</sup> while molecular species on  $\text{TiO}_2$  surface form reactive oxygen species (ROS).<sup>18</sup> Redox reactions of species on heterogeneous surfaces caused by electrons and holes play a major role in a number of chemical reactions of key importance from photocatalysis and electrochemistry to the damage of biological molecules and tissues<sup>18</sup>. ROS, such as  $\cdot\text{O}_2^-$ ,  $\text{O}_2^{2-}$ ,  $\text{H}_2\text{O}_2$ ,  $^1\text{O}_2$ ,  $\cdot\text{OH}$  on the insulating  $\text{TiO}_2$  catalyst, are among the most important on-surface molecular species<sup>18</sup>. Both ROS and SaQDs are stable well above the room temperature<sup>19</sup>.

Tuning of the redox states of ROS and SaQDs, preferably not at too low a temperature, can be provided by applying an appropriate bias voltage that facilitates an electron tunnelling between the oxygen atom and the tip of an atomic force microscope (AFM) or scanning tunnelling microscope (STM). The tuning efficiency is quantified by the electron tunnelling rates. However, the tunnelling processes are stochastic in nature and hence collecting sufficient statistics has so far been only possible at ultra-

low temperatures, when the AFM/STM system remains stable for sufficient time (low thermal drift)<sup>20–24</sup>.

Here we developed an alternative very fast experimental method, the Fast-Cycling Kelvin Probe Force Spectroscopy (KPFs), that enables one to collect required statistics over short times at which the system remains stable. Our method is based on driving bias voltage cycles at much higher speeds and thus enforcing the transitions to (stochastically) happen, thus effectively circumventing all the existing experimental limitations. That breakthrough enabled us to manipulate between redox states of multiple SaQDs on the  $\text{TiO}_2$  substrate at 78 K. The tunnelling rates acquired over a wide range of tip-sample distances and applied voltages provide unexpected insights into the electronic structure and correlation between the oxygen species on the  $\text{TiO}_2$  surface. In particular, we show that oxygen species of the same charge that appear identical in AFM imaging are clearly distinguished by our method; this effect is attributed to environmental effects which subtly change their electronic structure.

## Results and discussion

**AFM imaging and KPFM charge manipulation.** In our experiments, ROS and SaQDs were prepared by evaporating molecular oxygen on the rutile  $\text{TiO}_2(110)$  surface<sup>14</sup>. Molecular oxygen is known to form at low and room temperatures a combination of molecular and dissociative species randomly distributed on the surface<sup>9,19</sup>. Figure 1a shows an atomically resolved high-resolution

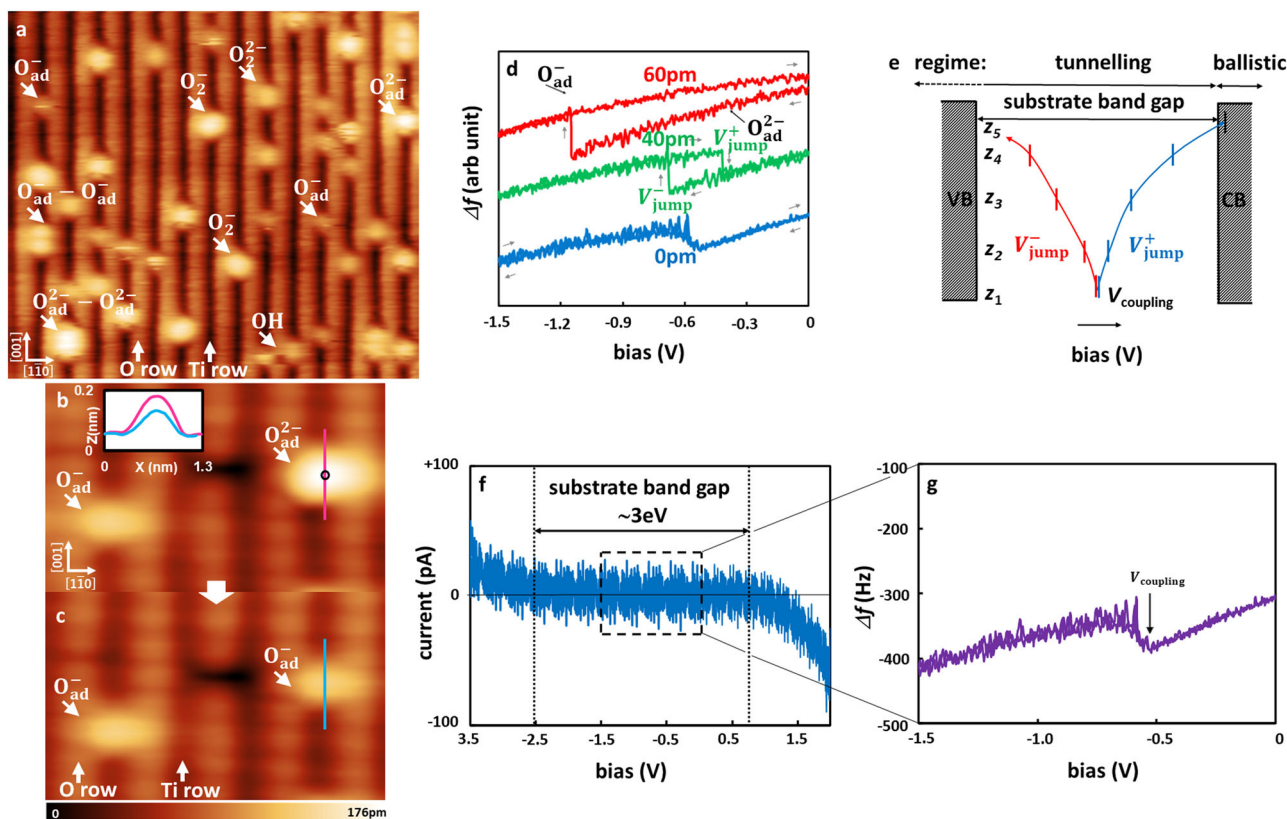


**Fig. 1** Various O atom species on the  $\text{TiO}_2$  surface and their charge manipulation at 78 K. **a** Large-scale image of the  $\text{TiO}_2$  surface showing different oxygen species identified by spectroscopy: adatoms  $\text{O}_{ad}^-$ ,  $\text{O}_{ad}^{2-}$ ; pairs of adatoms  $\text{O}_{ad}^{2-}-\text{O}_{ad}^-$ ,  $\text{O}_{ad}^- - \text{O}_{ad}^-$ ; molecules  $\text{O}_2^{2-}$  (peroxide),  $\text{O}_2^-$  (superoxide); and OH (hydroxyl group). High-resolution AFM images of an O atom before **(b)**, as  $\text{O}_{ad}^{2-}$  and after **(c)**, as  $\text{O}_{ad}^-$  charge manipulation. Inset in **(b)**: the corresponding line scans across the two species. **d** Results of typical KPFs manipulations with the tip positioned as indicated by a black circle in **(b)**, at three heights as indicated. Each such manipulation leads to image **(b to c)** transformation. **e** Schematic sketch of positions of the occupied  $\text{O}_2^-$   $p$ -orbitals responsible for the oxidation process ( $V_{jump}^-$ , full red lines) and of the unoccupied  $\text{O}^-$   $p$ -orbital responsible for the reduction process ( $V_{jump}^+$ , full blue lines) relative to the substrate band gap (VB/CB valence/conduction band) as a function of tip-sample distance ( $z_1 < z_2 < \dots < z_5$ ), and bias voltage. **f** Tunnelling current vs. bias voltage taken above  $\text{TiO}_2$  surface. **g** Frequency shift vs. bias voltage observed at close approach over an O atom, which is the same height as the blue curve in **d**.

AFM image measured at the bias (with respect to the sample)  $V_s = 0$  V, which exhibits all the major ROS species ( $O_2^-$ ,  $O_2^{2-}$ , OH), the atomic SaQDs species ( $O_{ad}^-$ ,  $O_{ad}^{2-}$ ), and pairs of atomic species ( $O_{ad}^-O_{ad}^-$ ,  $O_{ad}^{2-}O_{ad}^{2-}$ ). While all molecular ROS and atomic species are rarely seen in one image, as in Fig. 1a, many of them have been observed and assigned separately or in smaller combinations. Adatoms:  $O_{ad}^{2-}$ ,  $O_{ad}^-$  in addition to being subject of the present study were studied in ref. 25; pairs of adatoms:  $O_{ad}^{2-}O_{ad}^{2-}$ ,  $O_{ad}^-O_{ad}^-$  were studied in refs. 13,14,25; molecules:  $O_2^{2-}$  (peroxide) in ref. 14,  $O_2^-$  (superoxide), please see Supplementary Fig. S2, and OH hydroxyl defect was studied in ref. 26. Those previous assignments along with line profiles and image parameters in Supplementary note 3 and Supplementary Tab. SI give further support to the interpretation of the species in Fig. 1a. It has been shown<sup>13,14</sup> that the redox state of the ROS species can be switched by KPFS repeatedly and reversibly. While all the above ROS have been easily detected in aqueous suspensions<sup>18</sup>, the previous low-temperature AFM studies of on-surface oxygen atomic and molecular species in UHV have been controversial, interpreting them as all being only doubly charged<sup>9</sup>.

Figure 1b shows an atomically resolved AFM image of a SaQD. Two single bright spots of different sizes can be observed. Because of the careful surface preparation prior to oxygen exposure which results in samples that mostly contain oxygen vacancies on their surface (see Supplementary Fig. S1c), we are confident that the SaQD we observe must be adsorbed oxygen atoms in one of the two charge states: the small bright spot corresponding to  $O_{ad}^-$  and the big one to  $O_{ad}^{2-}$ . As argued in Supplementary notes 2 and 16 and Supplementary Fig. S14, the observed bright spots cannot be attributed to hydroxyls.

Figure 1c shows an identical area after a KPFS induced single-electron charge manipulation that transforms  $O_{ad}^{2-}$  into  $O_{ad}^-$ . In this experiment, the tip was manually brought above the  $O_{ad}^{2-}$  at the position indicated by the black circle in Fig. 1b and the sample bias was linearly lowered to  $-1.5$  V, while the frequency shift was observed to jump at  $V_{jump}^-$  as indicated in Fig. 1d. The jump in the frequency shift indicates that a single-electron tunneled from the O atom to the tip. The line scans across the O species (shown in the inset to panel b) clearly indicate that the charge on the O species is reduced from minus two to minus one. Therefore, the jump of the KPFS curve indicates a transformation of  $O_{ad}^{2-}$  into  $O_{ad}^-$  (oxidation) which forms a long-lived (meta)stable on-surface species (see Supplementary Fig. S7). On the reverse ramp direction, another jump in the frequency shift is observed at voltage  $V_{jump}^+$ , which corresponds to an electron tunnelling from the tip to the oxygen atom converting the latter back into the  $O_{ad}^{2-}$  state (reduction). The described procedure corresponds to a complete cycle which can be repeated at will on the same SaQD many times or performed consecutively on several SaQDs one after the other, see Supplementary Fig. S3.

The experiments repeated at various tip heights (see, e.g., Fig. 1d) show that on average the hysteresis window  $V_{jump}^- \leq V \leq V_{jump}^+$  is reduced as the tip is moved closer to the surface. At the lowest height, which was set as the zero-height reference set point, the hysteresis disappears completely indicating a very close near-contact regime in which electrons are tunnelling back and forth between the tip and the O atom.

The physics of the observed processes is quite simple. When the bias voltage is ramped in the negative direction, the  $O^{2-}$  atom  $p$  level is lifted, and as it comes close to the tip Fermi level, one electron from the  $O^{2-}$  tunnels into the tip whereby an  $O^-$  is formed with its singly occupied energy level being still within the gap and the opposite spin unoccupied energy level moving upwards. When the bias voltage is ramped in the opposite

direction, the unoccupied energy level of the O atom moves downwards and, when it comes close to the Fermi energy of the tip, an electron tunnels back from the tip to the  $O^-$  atom, restoring the double occupation. The positions in the bias voltage where these redox transitions (stochastically) happen are schematically shown for different tip-sample distances in Fig. 1e (for a DFT model, see Supplementary Fig. S12). Note that, at large tip-sample distances, the unoccupied  $p$ -orbital of the  $O^-$  species is likely pushed into the conduction band and the redox state manipulation can be switched from the tunnelling regime into ballistic regime (see below). In the opposite limit, at a short tip-sample distance and  $V_{coupling}$  bias, Fig. 1g, all oxygen  $p$ -levels collapse into one within the  $TiO_2$  gap and the redox transitions proceed smoothly without any jumps in frequency shifts, the blue curve in Fig. 1d.

The O adatom constitutes a SaQD as manifested in Fig. 1f–g. It is seen in panel f that  $TiO_2$  has a band gap of over 3 eV, and the frequency shift transition observed at near-contact regime and shown in panel g, demonstrates that the O atom highest occupied/lowest unoccupied  $p$  states, which are being manipulated, Fig. 1b, c, are in the middle of the  $TiO_2$  band gap.

However, the conductance properties of the O atoms in the two redox states are quite different, as shown in Fig. 2. In this experiment we ramped the bias to up to 3 V with the tip placed above either of the two O species,  $O_{ad}^-$  and  $O_{ad}^{2-}$ , located next to each other, see panels a, c. If in the case of the singly charged O atom (an open shell) the current steadily increases, panel b, the current measured above the doubly charged O species (a closed shell) remains around zero, panel d. The fact that the current increases steadily in the former case suggests that the unoccupied  $p$ -orbitals of  $O_{ad}^-$  are in the conduction band of the  $TiO_2$  substrate, and, hence, are delocalised and strongly hybridised with the substrate states (the ballistic transport regime). Hence, using AFM tip we are able to switch locally and repeatedly the oxygen atom on the surface between two conductance regimes: opened (binary 1 state) and locked (0 state).

Moreover, two such SaQDs can be frequently found as nearest pairs<sup>13</sup> or can be atomically tip-manipulated by voltage pulses along the Ti trenches or across the O rows, see Supplementary Fig. S3 and ref. 27, into the pairs or longer “wires”. The charge state of the pairs of atoms can be manipulated<sup>14</sup> to assume configurations akin to ferromagnetic (“1” “1”), non-magnetic (“0” “0”), or “chess board” or anti-ferromagnetic (“1” “0”). In this way one can create with AFM + KPFS a desired binary arrangement of 0's and 1's, a nanosymbol encoded by means of SaQDs on the surface, which can be read out/decoded either by AFM (distinguished by the size of the spots) or STM (by whether there is current or not) tip. This opens up an exciting possibility towards preparing devices by tip-tuning with distributed over the surface local regions of high and negligible atomic conductance of desired binary structure.

### Determination of electron tunnelling rates by KPFS measurement.

Both the on-surface electrochemistry of ROS as well as the encoding of binary information by SaQDs require tip-tuning of their quantum states, preferably not at too low a temperature. This ability is quantified by the tunnelling rates and, hence, measuring the tunnelling rates becomes of utmost importance. The rates depend crucially on the applied bias voltage and the tip height used; an exponential dependence on the tip height at large tip-sample distances and increase of discharging/recharging rate with the increase of the voltage in negative/positive direction, are expected. However, tunnelling processes are stochastic in nature and collecting sufficient statistics has so far been only possible at ultra-low temperatures<sup>16,20–23,28–31</sup> to ensure insignificant



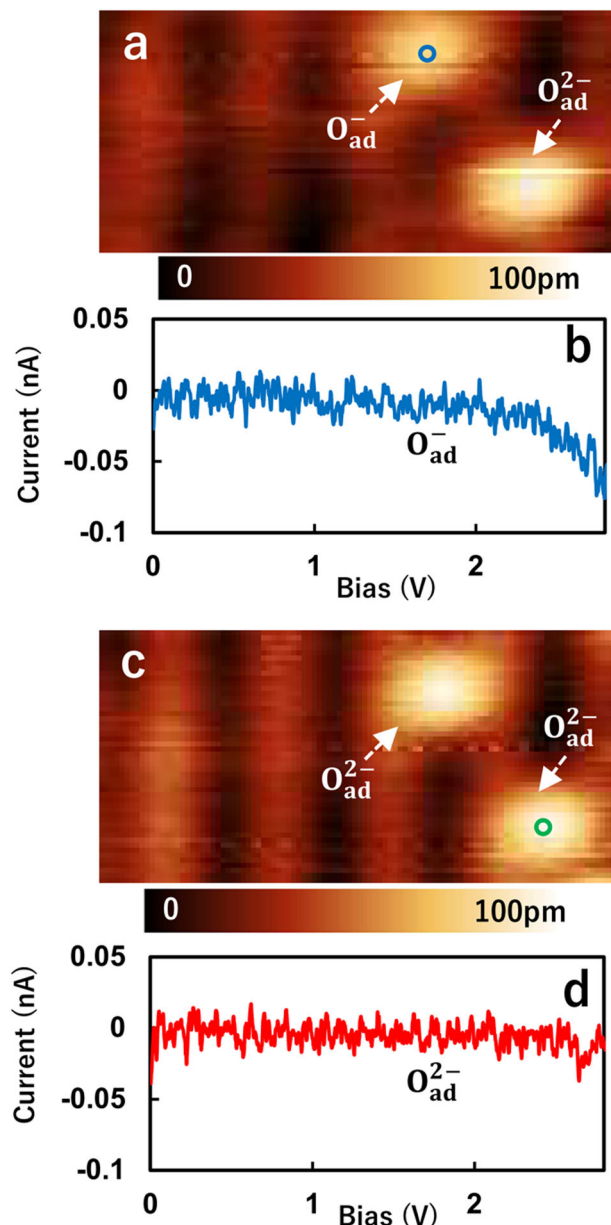


**Fig. 2 Measured  $O_{ad}$  conductance.** **a, c** AFM images of the  $TiO_2$  surface showing O atoms in both redox states prior to current measurements (the constant  $\Delta f$  mode, zero bias). This experiment was carried out at larger tip-sample distances than those used in Fig. 1 and at positive biases. **b** The current measured by placing the tip above the  $O_{ad}^-$  species as indicated by the dot in **(a)**. **d** The current measured by placing the tip above the  $O_{ad}^{2-}$  species as indicated by the dot in **(c)**. During the measurements, the feedback loop was switched off, and the sample bias was ramped from zero in the direction of the positive voltage.

temperature drift over the time of the measurement. For instance, measuring either the telegraph-noise current or frequency shift fluctuations), see Supplementary Fig. S6 (when transition rates of forward and reverse processes are comparable, Supplementary Fig. S5), or applying a specific time-dependent bias protocol consisting of 10 s cycles, each containing tip height change<sup>24</sup>, see Supplementary Fig. S7.

We propose an alternative approach, the Fast-Cycling KPFS method (FC-KPFS), in which we accelerate the transitions by a continuous cyclic driving process, at a fixed position of the tip, which forces the transitions of the redox state to (stochastically)

occur rather than wait for them to occur spontaneously, and apply it to the SaQD at 78 K. This can be done at much wider range of applied voltages and tip-sample distances and, because of the acceleration by the driven system dynamics by over an order of magnitude, see Supplementary Fig. S11, at much higher temperatures. This method does not require the transition rates in both directions be comparable.

The experimental protocol is illustrated in Fig. 3. During each cycle the frequency shift jumps happen stochastically at different values of the bias voltages  $V_{jump}^{\pm}$  that form discharging and recharging distributions. Analytical theory in Supplementary note 18 shows that the tunnelling rate (for a given tip height set point  $z_0$  and transition type) is described by the following exact formula:

$$\tilde{R}(t) = \tilde{P}(t) / \left( 1 - \int_0^t \tilde{P}(\tau) d\tau \right) \quad (1)$$

enabling one to determine the averaged rate from the experimentally acquired probability density  $\tilde{P}(t)$ . The time dependence of the rate,  $\tilde{R}(t)$ , arises due to its dependence on the voltage,  $V(t) = \pm vt + V_0$ , changing linearly with time when it is ramped either in the negative or positive directions. Hence, we can obtain a physically meaningful oscillation-averaged rate as a function of the voltage,  $R(V)$ . By running the ramping at faster speeds  $v$  enables collecting more statistical data within the time the system remains stable. Even though the probability density depends on  $v$ , the rate  $R(V)$  does not (Supplementary Figs. S11, S15).

Measured recharging and discharging probability density distributions for five values of the tip height set points collected at one arbitrarily selected SaQD are shown as histograms in Fig. 4a–e. In order to extract smooth dependencies of the rate on the bias voltage, Fig. 4f, we devised a reverse engineering Monte Carlo (MC) based procedure, see Supplementary note 19, and Supplementary Figs. S15–S18. The MC-based probability densities are shown by full lines in Fig. 4a–e. Both discharging and recharging rates increase rapidly with the bias that is changing in the appropriate direction. Surprisingly, at small distances between 0 and 30 pm the decrease with  $z$  is not exponential, Fig. 4g, h, where we show the logarithm of  $R$  as a function of the tip-sample distance. These results indicate that the height decay rate  $\beta = -\frac{d}{dz} \ln R$  is not a constant at small, but becomes such at larger tip-sample distances, as expected for an ordinary tunnelling regime, see also Supplementary note 20. That analysis also suggests, that tunnelling will proceed mainly around the lower turning point of the cantilever oscillation, and, hence, the extracted rates  $R(z, V)$  will effectively correspond to the physical tunnelling rates  $r(z, V)$  at the lowest tip-sample distance, especially at low oscillation amplitudes (extraction of  $r(z, V)$  from the averaged rates is discussed in Supplementary note 20 and the approximate WKB theory in Supplementary note 21 and Supplementary Fig. S19).

**New insight into electronic structure of SaQDs.** So, our method enables one to measure oscillation-averaged tunnelling rates between the SaQD and the AFM tip at a wide range of tip-sample distances and applied bias voltages, and these measurements do not need to be performed at very low temperature as the sufficient statistics can be acquired over very short times during which the system remains stable. Moreover, due to increased efficiency, we have been able to apply our method to many O atoms adsorbed on the surface. Comparing results of these measurements we discovered, quite unexpectedly, that our method performs as a sensitive probe in distinguishing different O species on the surface otherwise appearing identical in AFM/KPFS measurements. As shown in Supplementary Figs. S6, S8, S9, SaQDs with identical AFM images exhibit distinctly different electronic properties

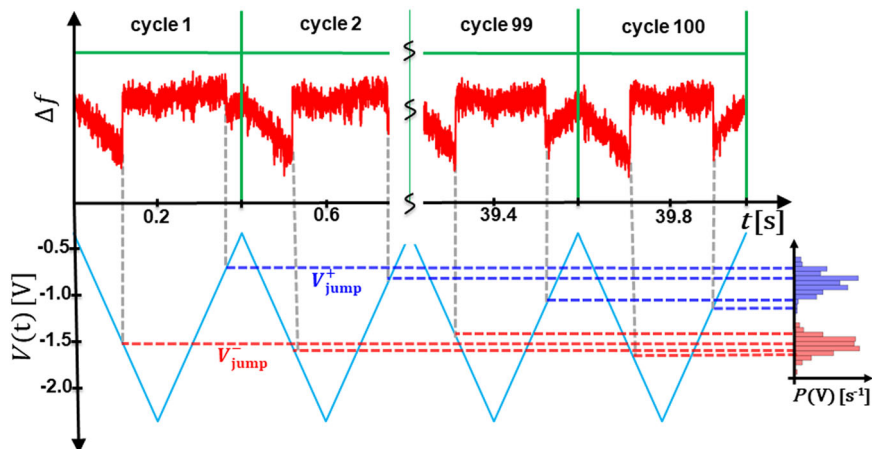


**Fig. 3 FC-KPFS protocol.** Time variations of the frequency shift  $\Delta f$  due to the bias voltage ramps shown below. Solid green vertical lines separate complete cycles, while dashed blue and red lines indicate voltages  $V_{jump}^+$  and  $V_{jump}^-$  at which frequency shift jumps happen. Acquired values of the  $V_{jump}^+$  and  $V_{jump}^-$  voltages form, correspondingly, recharging (blue) and discharging (red) distributions shown on the right.

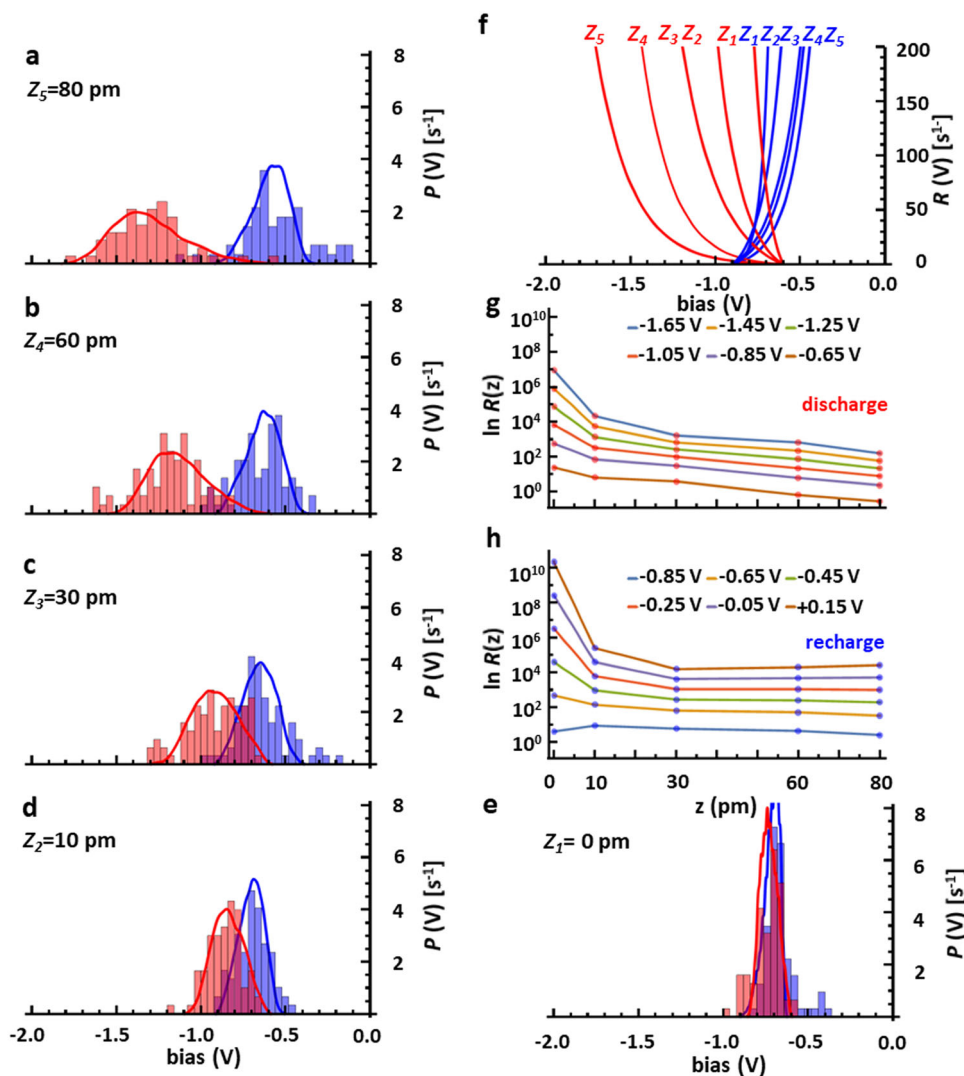


**Fig. 4 FC-KPFS measured and simulated probability density distributions and tunnelling rates at 78 K.** **a-e** Measured histograms of the probability density distributions for recharging (blue) and discharging (red) tunnelling transitions at several tip heights as indicated. Solid red and blue lines show MC simulated distributions which provide the best fit to the measured ones. **f** Optimised transition rates vs. bias for the five tip heights. **g, h**  $\ln R$  as a function of  $z$  for discharging and recharging, respectively.

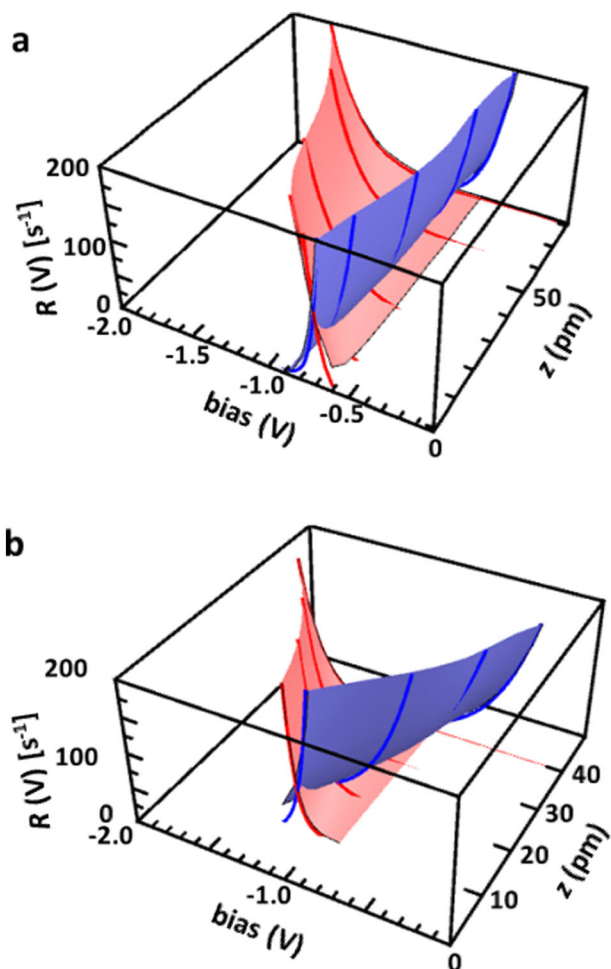


**Fig. 5 Full characterisation of electron tunnelling for two different dots. a, b** 3D graphs of the recharge (blue)/discharge (red) rates as a function of both the bias, V, and the tip-height,  $z$ , for two different SaQDs. **a** Corresponds to the data in Fig. 4, for the data in **(b)**, see Supplementary Fig. S9.

revealed by tunnelling rate measurement. In Fig. 5 we compare 3D plots of tunnelling rates  $R(z, V)$  as a function of both  $z$  and  $V$  collected on two different SaQDs measured with identical or very similar tips, see Supplementary Fig. S10. (i) A stronger bias dependence for recharging than discharging rates for the two dots is seen in Fig. 5a for one dot, whereas the results for another in Fig. 5b suggest the opposite behaviour. We attribute these qualitatively different behaviours to two different types of SaQDs on the surface, rather than to differences in the tip structure (for results obtained with a different tip structure, see Supplementary Fig. S8), as the latter we expect may only affect the rates quantitatively. (ii) The tunnelling rates differ by several orders of magnitude for identical tip-sample distances and bias voltages. (iii) Threshold biases at which the charging and discharging processes initiate differ by up to 0.5 V.

As the environments of the target SaQDs are not equivalent, see the bottom of Supplementary Fig. S10, and the close oxygen adatoms are electronically coupled on the surface, Supplementary Fig. S13, we attribute this tunnelling behaviour to differences in the local environment of the SaQDs, such as presence (or not) of surface and subsurface defects or nearby oxygen adatoms. As the latter are charged (either as  $\text{O}_{ad}^-$  or  $\text{O}_{ad}^{2-}$ ), each O species experiences a unique electrostatic potential affecting its electronic properties. Subsurface defects, such as Ti interstitials, can also impact the electrostatic profile of surface species. Hence, differences

in behaviour of tunnelling rates of electrons in switching the redox states of SaQDs indicate presence of electronically inequivalent SaQDs. Since AFM images of two SaQDs in an identical redox state are virtually identical, Supplementary Fig. S6, we conclude that the tunnelling rates serve as a much more sensitive probe of the SaQDs than the AFM images.

## Conclusion

In conclusion, we studied oxygen species on the rutile  $\text{TiO}_2$  surface at 78 K in the form of SaQDs and ROS molecules using atomic force microscopy. We have shown that KPFS can readily tune the redox state of all those atomic and molecular species between minus one and minus two, thereby switching the conductivity through this tip-tunable two-state SaQD device between the opened (“1”) or locked (“0”) states. The switching can be done reversibly and repeatedly; moreover, as demonstrated in a separate experimental run shown in Supplementary Fig. S4, switching of O adatoms can be performed consecutively, one O adatom after another, suggesting, in combination with atom manipulation capability (Supplementary Fig. S3 and ref. 27), a lego-type two-dimensional nano-building blocks method. In particular, the charge state of pairs or assemblies of oxygen adatoms can be manipulated to assume configurations akin to ferro- or anti-ferromagnetic and thus, by means of an appropriate on-surface distribution of SaQDs, encoding a desired binary arrangement of 0’s and 1’s on the surface. The fact that adatoms on the rutile  $\text{TiO}_2$  surface can easily be atomically tip-manipulated<sup>27</sup> opens up the intriguing possibility of *à la carte* preparation of SaQDs with desired electronic properties.

A possible complication with device use of the oxide materials is their long-time stability. Experimentally, at liquid nitrogen temperatures, the various oxygen species could only be established for time periods of a few dozen minutes. Hence, ultra-low temperatures would be required to stabilise them over longer time periods. The oxide systems are also heavily impacted by the defects which are known to interfere with each other. Surface and subsurface defects can donate electrons to the  $\text{TiO}_2$  which can eventually recombine with the on-surface charged oxygen species. The dynamics of those processes could again be slowed down by ultra-low temperatures.

The tuning efficiency of the on-surface oxygen species and nano-devices has been quantified using our fast-cycling-KPFS method based on driven system dynamics that is faster than any alternative method by, at least, an order of magnitude. Hence, if properties of the oxide materials at and above liquid nitrogen temperatures are of interest, the FC-KPFS method becomes indispensable and, due to the experimental speedup, is expected to be superior at all temperatures. The measured electron tunnelling rates uncovered environment-related differences in the electronic structure of the oxygen species which remain hidden in the customary AFM microscopy.

## Methods

The experiments were carried out using a low-temperature ultrahigh vacuum AFM system. The deflection of the cantilever was measured using the optical beam deflection method. The base pressure was lower than  $5.0 \times 10^{-11}$  Torr. The temperature of the AFM unit was kept at liquid nitrogen temperature (78 K). The AFM measurements were performed in the frequency modulation detection mode. The cantilever was oscillated at the resonance frequency keeping the oscillation amplitude constant.

The rutile  $\text{TiO}_2(110)-(1 \times 1)$  sample, see the Supplementary Fig. S1, was prepared by sputtering and annealing to 900 K in several cycles. The sample was exposed to oxygen at room temperature for 0.5 L and then transferred to a measurement chamber precooled to 78 K.

The atom tracking method was used to compensate the thermal drift between the tip and surface during the measurements. dc bias voltage was applied to the sample in KPFS measurements or charge manipulation and a periodic saw tooth bias, typically in the region (0, -2) V in the discharge cycle and (-2, 0) V in the recharge



cycle. We used a Ir-coated Si cantilever (Nano sensors SD-T10L100,  $f_0 = 800$  kHz,  $A = 500$  pm). Metal Ir tips provide stable AFM imaging compared to the bare Si tip. The tip was initially annealed to 600 K and then cleaned by Ar<sup>+</sup> ion sputtering to remove the contamination before experiments. The PLL bandwidth is 100 Hz, which is large enough for the purpose of our FS-KPFS experiments. The AFM operating condition corresponds to the hole mode<sup>13</sup>, see also Supplementary note 2.

More details of the electronic structure calculations, Monte Carlo simulations of the experiments, and the underlying stochastic theory of the experiment are given in Supplementary Note 12.

### Data availability

All experimentally generated raw data (text files), such as AFM images, KPFS charging/discharging hysteresis loops, probability density distributions, reverse Monte Carlo processing, as well as results of electronic structure simulations (geometry files) are available from the corresponding authors upon reasonable request.

Received: 24 November 2020; Accepted: 10 June 2021;

Published online: 01 July 2021

### References

- Diebold, U. The surface science of titanium dioxide. *Surf. Sci. Rep.* **48**, 53–229 (2003).
- Thompson, T. L. & Yates, J. Surface science studies of the photoactivation of TiO<sub>2</sub> new photochemical processes. *Chem. Rev.* **106**, 4428–4453 (2006).
- Pang, C. L., Lindsay, R. & Thornton, G. Chemical reactions on rutile TiO<sub>2</sub>(110). *Chem. Soc. Rev.* **37**, 2328–2353 (2008).
- Yates Jr., J. T. Photochemistry on tio<sub>2</sub>: Mechanisms behind the surface chemistry. *Surf. Sci.* **603**, 1605–1612 (2009).
- Dohnálek, Z., Lyubintsev, I. & Rousseau, R. Thermally-driven processes on rutile TiO<sub>2</sub>(110)-(1 × 1): A direct view at the atomic scale. *Prog. Surf. Sci.* **85**, 161–205 (2010).
- Henderson, M. A. & Lyubintsev, I. Molecular-level insights into photocatalysis from scanning probe microscopy studies on TiO<sub>2</sub>(110). *Chem. Rev.* **113**, 4428–4455 (2013).
- Guo, Q. et al. Elementary photocatalytic chemistry on TiO<sub>2</sub> surfaces. *Chem. Soc. Rev.* **45**, 3701–3730 (2016).
- Setvin, M., Hulva, J., Parkinson, G. S., Schmid, M. & Diebold, U. Electron transfer between anatase TiO<sub>2</sub> and an O<sub>2</sub> molecule directly observed by atomic force microscopy. *Natl. Acad. Sci. U.S.A.* **114**, E2556–E2562 (2017).
- Sokolović, I. et al. Resolving the adsorption of molecular O<sub>2</sub> on the rutile TiO<sub>2</sub>(110) surface by noncontact atomic force microscopy. *Proc. Natl. Acad. Sci. U.S.A.* **117**, 14827–14837 (2020).
- Dagdeviren, O. E. et al. Ergodic and nonergodic dynamics of oxygen vacancy migration at the nanoscale in inorganic perovskites. *Nano Lett.* **20**, 7530–7535 (2020).
- Liu, Y. et al. Hysteretic ion migration and remanent field in metal halide perovskites. *Adv. Sci.* **7**, 2001176 (2020).
- Wendt, S. et al. The role of interstitial sites in the Ti<sub>3d</sub> defect state in the band gap of titania. *Science* **320**, 1755–1759 (2008).
- Zhang, Q. Z. et al. Measurement and manipulation of the charge state of adsorbed oxygen adatom on rutile TiO<sub>2</sub>(110)-1 × 1 surface by nc-AFM and KPFM. *J. Am. Chem. Soc.* **140**, 15668 (2018).
- Adachi, Y. et al. Tip-induced control of charge and molecular bonding of oxygen atoms on the rutile TiO<sub>2</sub>(110) surface with atomic force microscopy. *ACS Nano* **13**, 6917–6924 (2019).
- Haider, M. B. et al. Controlled coupling and occupation of silicon atomic quantum dots at room temperature. *Phys. Rev. Lett.* **102**, 046805 (2009).
- Taucer, M. et al. Single-electron dynamics of an atomic silicon quantum dot on the H-Si(001)-(2 × 1) surface. *Phys. Rev. Lett.* **112**, 256801 (2014).
- Huff, T. et al. Binary atomic silicon logic. *Nature Electr.* **1**, 636–643 (2018).
- Nosaka, Y. & Nosaka, A. Y. Generation and detection of reactive oxygen species in photocatalysis. *Chem. Rev.* **117**, 11302–11336 (2017).
- Lira, E. et al. Dissociative and molecular oxygen chemisorption channels on reduced rutile TiO<sub>2</sub>(110): an STM and TPD study. *Surf. Sci.* **604**, 1945–1960 (2010).
- Liljeroth, P., Repp, J. & Meyer, G. Current-induced hydrogen tautomerization and conductance switching of naphthalocyanine molecules. *Science* **317**, 1203 (2007).
- Pana, S. et al. Design and control of electron transport properties of single molecules. *Proc. Natl. Acad. Sci. U.S.A.* **106**, 15259–15263 (2009).
- Auwärter, W. et al. A surface-anchored molecular four-level conductance switch based on single proton transfer. *Nat. Nanotechnol.* **7**, 41 (2012).
- Kumagai, T. et al. Controlling intramolecular hydrogen transfer in a porphycene molecule with single atoms or molecules located nearby. *Nat. Chem.* **6**, 41 (2014).
- Fatayer, S. et al. Reorganization energy upon charging a single molecule on an insulator measured by atomic force microscopy. *Nat. Nanotechnol.* **13**, 376–380 (2018).
- Wen, H. F., Sang, H., Sugawara, Y. & Li, Y. J. Imaging oxygen molecular adsorption and dissociation on the Ti site of rutile TiO<sub>2</sub>(110) surface with real configuration at 78 K by atomic force microscopy. *Phys. Chem. Chem. Phys.* **22**, 1975–19801 (2020).
- Wen, H. F. et al. Identification of atomic defects and adsorbate on rutile TiO<sub>2</sub>(110)-(1 × 1) surface by atomic force microscopy. *J. Phys. C* **42**, 25756–25760 (2019).
- Zhang, Q. et al. Electrical engineering of the oxygen adatom and vacancy on rutile TiO<sub>2</sub>(110) by atomic force microscopy at 78 K. *J. Phys. Chem. C* **123**, 28852–28858 (2019).
- Donhauser, Z. J. et al. Conductance switching in single molecules through conformational changes. *Science* **292**, 2303 (2001).
- Jia, C. et al. Covalently bonded single-molecule junctions with stable and reversible photoswitched conductivity. *Science* **352**, 1443 (2016).
- Meng, L. et al. Side-group chemical gating via reversible optical and electric control in a single molecule transistor. *Nat. Commun.* **10**, 1 (2019).
- Kocić, N. et al. Periodic charging of individual molecules coupled to the motion of an atomic force microscopy tip. *Nano Lett.* **15**, 4406–4411 (2015).

### Acknowledgements

This work was supported by a Grant-in-Aid for Scientific Research from Japan Society for the Promotion of Science (JSPS) from the Ministry of Education, Culture, Sports, Science, and Technology of Japan (JP16H06327, JP16H06504 and JP17H01061). This work was also supported by the International Joint Research Promotion Program of Osaka University (J171013014, J171013007 and Ja19990011). This project was supported by the National Natural Science Foundation of China (NSFC) [JSPS-NSFC(J191053055)]. We acknowledge the support by APVV-18-0211 and VEGA-2/0123/18, VEGA-2/0125/20 VEGA-2/0070/21 projects. We also gratefully acknowledge Center for Computational Materials Science, Institute for Materials Research, Tohoku University for the use of MASAMUNE-IMR supercomputer. L.K. acknowledges useful discussions with Anatoly Zayats (a.zayats@kcl.ac.uk) and Sergi Garcia-Manyes (sergi.garcia-manyes@kcl.ac.uk).

### Author contributions

Y.A., J.B., H.F.W., Q.Z., M.M., S.T., Y.S., H.S., Y.J.L., I.S. and L.K. designed the experiments. Y.A., H.F.W., Q.Z., M.M. performed the experiments. Y.A., J.B., H.F.W., Q.Z., M.M., S.T., Y.S., H.S., Y.J.L., I.S. and L.K. analyzed the data. J.B., S.T., I.S. and L.K. conducted the theoretical calculations. Y.J.L., Y.S., I.S. and L.K. directed the project. All authors discussed the results and wrote the manuscript.

### Competing interests

The authors declare no competing interests.

### Additional information


**Supplementary information** The online version contains supplementary material available at <https://doi.org/10.1038/s43246-021-00176-5>.

**Correspondence** and requests for materials should be addressed to Y.L., I.S. or L.K.

**Peer review information** *Communications Materials* thanks the anonymous reviewers for their contribution to the peer review of this work. Primary Handling Editors: Aldo Isidori.

**Reprints and permission information** is available at <http://www.nature.com/reprints>

**Publisher's note** Springer Nature remains neutral with regard to jurisdictional claims in published maps and institutional affiliations.

 **Open Access** This article is licensed under a Creative Commons Attribution 4.0 International License, which permits use, sharing, adaptation, distribution and reproduction in any medium or format, as long as you give appropriate credit to the original author(s) and the source, provide a link to the Creative Commons license, and indicate if changes were made. The images or other third party material in this article are included in the article's Creative Commons license, unless indicated otherwise in a credit line to the material. If material is not included in the article's Creative Commons license and your intended use is not permitted by statutory regulation or exceeds the permitted use, you will need to obtain permission directly from the copyright holder. To view a copy of this license, visit <http://creativecommons.org/licenses/by/4.0/>.

© The Author(s) 2021